Multipeak envelope of the above-threshold-ionization energy spectrum in a strong circularly polarized laser field

Jarosław H. Bauer*
Katedra Fizyki Teoretycznej Uniwersytetu Łódzkiego, Ul. Pomorska 149/153, PL-90-236 Łódź, Poland
(Received 29 March 2012; published 28 June 2012)

We develop a well-known strong-field approximation in the length gauge for a two-dimensional model atom in a strong circularly polarized laser field. For excited initial states (with the principal quantum number $n = 2$) outgoing photoelectrons usually show energy spectra with an envelope having two or three peaks: one always below and one always above the ponderomotive energy U_P. In contrast, for the ground state (with $n = 1$) there is always a single peak near U_P. Our numerical calculations show that the multipeak effect appears for sufficiently high laser intensities I and is more pronounced for higher laser frequencies ω. We believe that the field parameters ω and I, for which the multipeak envelope in the energy spectrum of above-threshold ionization exists, will enable its experimental observation in the near future.

DOI: 10.1103/PhysRevA.85.063417 PACS number(s): 32.80.Rm, 33.20.Xx, 33.60.+q, 33.80.−b

I. INTRODUCTION

Let us consider a light charged classical (point) particle initially moving steadily along a circular orbit around a center of the Coulomb force (a motionless heavy particle with an opposite electric charge). Suppose that an incoming electromagnetic plane wave propagates in the direction perpendicular to the plane of the circular orbit. Let the electromagnetic field be circularly polarized (CP). If the motion of the light particle is nonrelativistic, one can forget (this is an approximation) about the magnetic-field component of the Lorentz force coming from the plane wave. Furthermore, if one also neglects a light pressure (a momentum carried by light) the Lorentz force of the CP field is acting as a vector of a constant length F, rotating with a constant frequency. A motion of the light particle is determined by two forces: the latter one (which depends only on time) and the above-mentioned Coulomb force (which depends only on a position of the particle). One can imagine two physically different situations: initially the charged particle could rotate in the same or in the opposite direction with respect to the rotation of the electric-field vector of the incoming plane wave. In other words, along the propagation axis, angular momentum components of the particle and the field could have the same or opposite signs. Therefore, one should expect a different behavior of the particle in these two cases. In both situations the motion would remain in the initial plane of motion, because there is no force perpendicular to the plane. Classical equations of motion for this problem might be solved only numerically. However, if F (times the charge) is of the order of the initial Coulomb force or even greater, one can expect that the initial trajectory will be destroyed, and the light particle will run away from the Coulomb center. Far away from it, in the moving frame of reference, the light particle will move clockwise or anticlockwise (according to a helicity of the CP electromagnetic field).

Although electrons are not classical particles, manifestations of a classical dynamics should be present in an ionization of atoms and molecules in intense laser fields. Indeed, according to classical considerations [1,2], in strong CP laser fields, ionized electrons should have a kinetic energy peak (in Ref. [2] the kinetic energy that we mean is called "the drift energy") near its ponderomotive energy U_P (the latter is a result of an interaction of a free electron with the electromagnetic field). In the present work we will use atomic units (a.u.): $\hbar = e = m_e = 1$, and we will substitute explicitly -1 for the electronic charge (with the exception of Appendix C, where we will use cgs units). In such units $I = 2F^2$ (1 a.u. $\cong 3.51 \times 10^{16}$ W/cm^2) and $U_P = F^2/(2\omega^2)$ for the CP field. In any real above-threshold (ATI) [3] experiment, the situation is more complicated, because one deals with a laser pulse, where the frequency has some finite spectral width, and one also has to average over various intensities. Among models describing ATI, S-matrix theories [4–7], sometimes also called the strong-field approximation (SFA) [7], are significant. The latter may be applied in the length gauge (LG) [4,8] or in the velocity gauge (VG) [7]. Extensive studies of gauge aspects by others [9–13] as well as by us [8,14–17] has led us to a present belief of superiority of the LG in the context of S-matrix and strong laser fields. Our present results amplify this conviction.

This work is organized as follows. In Sec. II we develop the SFA in two spatial dimensions for the CP laser field in both gauges. In Sec. III we present results of our numerical calculations with regard to photoelectron energy spectra from the ionization of an atom with the principal quantum number $n = 1$ or $n = 2$ in the initial state. Discussion and conclusions are given in Sec. IV. In Appendix A we describe details of our analytical and numerical LG calculations. In Appendix B we describe such details of our VG calculations. In Appendix C we give chapter and verse of the superiority of the above-mentioned LG formulation of the SFA (for more details see Ref. [16], and references therein).

II. LG SFA IN TWO DIMENSIONS

In the present work we assume that a one-electron atom is placed in the intense plane-wave laser field such that $U_P \gg E_B$ (the binding energy of the atom in its initial state), but the electronic motion is nonrelativisic and one can drop

*bauer@uni.lodz.pl

 ©2012 American Physical Society

the magnetic-field component of the laser (i.e., one can use the dipole approximation; for the justification see, e.g., Ref. [18]). If the field is CP, as we assume throughout this work, the effect of the Coulomb potential on the final state of the outgoing electron should indeed typically be very small. The azimuthal dipole selection rule $\Delta m = \pm 1$ forces the angular momentum quantum number l to increase steadily during excitation of the real three-dimensional (3D) atom by the CP light [3]. A similar effect is present in the two-dimensional (2D) simpler model and the CP light, and we assume that the typical number of photons absorbed is large ($N \gg 1$). Therefore, here we use nonrelativisic Gordon-Volkov wave functions [19,20] as final states of the ionized electron. Instead of the hydrogen atom, we consider its 2D model [21], but with the same Coulomb potential $V(\vec{r}) = -Z/r$ (r is the distance from the nucleus with the electric charge Z). The advantage of this 2D model in a context of the ionization in strong laser fields is a possibility of being tested numerically by the very accurate and efficient alternate-direction implicit algorithm [22] (we plan to continue this task in the future). Moreover, as follows from the present work, the 2D ATI energy spectra qualitatively look very similar to analogous spectra in the polarization plane of the 3D ATI. In the real experiment most electrons are emitted in the polarization plane.

The laser field is described by the following vector potential:

$$\vec{A}(t) = \frac{a}{\sqrt{2}}[\hat{x}\,\cos(\omega t + \varphi_0) \pm \hat{y}\,\sin(\omega t + \varphi_0)], \tag{1}$$

where $\hat{x}$ and $\hat{y}$ are unit vectors along the respective axes, φ_0 is an arbitrary initial phase, and the electric field is given by $\vec{F}(t) = -(1/c)(\partial\vec{A}/\partial t)$. The signs $\pm$ correspond to the right and the left circular polarization, respectively. After Keldysh's and Reiss' examples, let us introduce the following intensity parameters γ [4], z, and z_1 [7], such that

$$\gamma = \frac{\omega\sqrt{2E_B}}{F}, \tag{2}$$

$$z = \frac{U_P}{\omega} = \frac{a^2}{4c^2\omega} = \frac{I}{4\omega^3} = \frac{F^2}{2\omega^3}, \tag{3}$$

$$z_1 = \frac{2U_P}{E_B} = \frac{F^2}{\omega^2 E_B} = \frac{2}{\gamma^2}. \tag{4}$$

We refer the reader to Refs. [4,7] or our work [14] (Secs. III–V therein) for more details about the SFA and its basic assumptions. For all calculations presented here $\gamma \ll 1$ and $z_1 \gg 1$. A general expression describing the ionization probability amplitude in the LG SFA is

$$\begin{aligned}(S-1)_{fi}^{\mathrm{LGSFA}} = i\int_{-\infty}^{\infty} dt\,\tilde{\Phi}_i\left(\vec{p} + \frac{1}{c}\vec{A}(t)\right) \\ \times\left[\frac{1}{2}\left(\vec{p} + \frac{1}{c}\vec{A}(t)\right)^2 + E_B\right] \\ \times \exp\left[\frac{i}{2}\int_{-\infty}^{t}\left(\vec{p} + \frac{1}{c}\vec{A}(\tau)\right)^2 d\tau + iE_B t\right],\end{aligned} \tag{5}$$

where $\vec{p}$ is the asymptotic momentum of the ionized electron [$\vec{p} = (p_x, p_y) = (p\,\cos\phi, p\,\sin\phi)$], and $\tilde{\Phi}_i(\vec{p})$ is the initial-state wave function (a bound state) in the momentum representation

$$\tilde{\Phi}_i(\vec{p}) = \int \frac{d^2r}{2\pi}\exp(-i\vec{p}\vec{r})\Phi_i(\vec{r}). \tag{6}$$

$\Phi_i(\vec{r})$ is a solution to the following eigenvalue equation ($r = |\vec{r}|$):

$$\left(-\frac{1}{2}\nabla^2 - \frac{Z}{r}\right)\Phi(\vec{r}) = E\Phi(\vec{r}), \tag{7}$$

with the total energy $E = E_n$ and

$$E_n = -\frac{Z^2}{2(n-1/2)^2}, \quad \text{for} \quad n = 1,2,3,\ldots. \tag{8}$$

In Eq. (5) we assume that $\lim_{t\to\pm\infty}\vec{A}(t) = \vec{0}$. Instead of a well-known three (omitting spin) quantum numbers (n,l,m) for the 3D atom, here we have only two quantum numbers (n,l) for the 2D atom. n is a principal quantum number, and l is an orbital quantum number such that $l = -(n-1), -(n-2), \ldots, -1, 0, 1, \ldots, (n-1)$. There are analytic solutions to Eq. (7), for both positive and negative E, in Ref. [21]. In Appendix A we give expressions for bound states ($E = -E_B < 0$) with $n = 1$ and $n = 2$. There is the ground state with (n,l) = (1,0) and the first excited state, which is triply degenerated: (n,l) = (2, −1), (2,0), and (2,1). A formula for the energy of bound states [Eq. (8)] is similar to its 3D counterpart $-Z^2/(2n^2)$ and depends only on the principal quantum number n. However, for the same Z, the 2D energy has a greater absolute value. For $Z = 1$ one has $E_1 = -0.5$ in three dimensions and $E_1 = -2.0$ in two dimensions.

To calculate the ionization probability amplitude (5) we proceed in the way applied already in Refs. [8,14]. There are three time-dependent factors in the main integrand upon time. (The integral in the exponential factor can be easily calculated analytically.) Each of them is time periodic with the period equal to a laser cycle. We expand the product of the first two factors in the first Fourier series

$$\begin{aligned}&\tilde{\Phi}_i\left(\vec{p} + \frac{1}{c}\vec{A}(t)\right)\left[\frac{1}{2}\left(\vec{p} + \frac{1}{c}\vec{A}(t)\right)^2 + E_B\right] \\ &\quad = \sum_{k=-\infty}^{\infty} A_k(\vec{p})\exp[ik(\omega t + \varphi_0 \mp \phi)],\end{aligned} \tag{9}$$

because this product is a function of

$$\frac{1}{2}\left(\vec{p} + \frac{1}{c}\vec{A}(t)\right)^2 = \frac{p^2}{2} + z\omega + \sqrt{2z\omega}p\,\cos(\omega t + \varphi_0 \mp \phi). \tag{10}$$

The third factor in Eq. (5) we expand in the second Fourier series

$$\begin{aligned}&\exp\left[\frac{i}{2}\int_{-\infty}^{t}\left(\vec{p} + \frac{1}{c}\vec{A}(\tau)\right)^2 d\tau + iE_B t\right] \\ &\quad = e^{iC}\sum_{n=-\infty}^{\infty} J_n\left(\sqrt{\frac{2z}{\omega}}p\right)\exp\left[i\left(\frac{p^2}{2} + z\omega + E_B + n\omega\right)t\right. \\ &\qquad \left. + in(\varphi_0 \mp \phi)\right].\end{aligned} \tag{11}$$

In Eq. (11) we put into use the well-known Fourier-Bessel expansion with the ordinary Bessel functions $J_n(x)$ (below x and y are any real numbers),

$$\exp(ix\sin y) = \sum_{n=-\infty}^{\infty} J_n(x)\exp(iny). \tag{12}$$

The phase factor e^{iC} (C is some real number, constant in time) will be dropped next because, in the end, only $|(S-1)_{fi}^{\mathrm{LGSFA}}|^2$ matters. Utilizing Eqs. (9) and (11) in Eq. (5) we obtain

$$\begin{aligned}(S-1)_{fi}^{\mathrm{LGSFA}} = 2\pi i \sum_{N,k=-\infty}^{\infty} & A_k(\vec{p})J_{N-k}\left(\sqrt{\frac{2z}{\omega}}p\right) \\ & \times \exp[iN(\varphi_0 \mp \phi)] \\ & \times \delta\left(\frac{p^2}{2} + z\omega + E_B + N\omega\right),\end{aligned} \tag{13}$$

where instead of n we set $N = n + k$, and we have adopted the well-known representation of the Dirac δ function: $\delta(E) = (2\pi)^{-1}\int_{-\infty}^{\infty}\exp(iEt)dt$. The differential ionization rate $\gamma(\vec{p})$, which is the transition probability per unit time and unit volume in the $\vec{p}$ space, can be found from

$$\gamma(\vec{p}) = \lim_{t\to\infty}\frac{|(S-1)_{fi}|^2}{t}. \tag{14}$$

To obtain the total ionization probability per unit time Γ, we integrate the differential ionization rate over all the possible final momenta of the outgoing electron

$$\Gamma^{\mathrm{LGSFA}} = \int d^2p\,\gamma(\vec{p}) = \sum_{N=N_0}^{\infty}\Gamma_N, \tag{15}$$

where the number N is a multiphoton order and $N_0 = [z + E_B/\omega] + 1$ may be treated as a minimal number of photons absorbed. (Here the symbol $[x]$ denotes the integer part of the number x.) The final kinetic energy E_N of the ionized outgoing electron is quantized according to the following formula:

$$E_N = p_N^2/2 = N\omega - z\omega - E_B. \tag{16}$$

Consecutive terms Γ_N form the ATI energy spectrum, if we plot a curve connecting the points (E_N,Γ_N) in the OXY plane. These points are in a sequence separated by the photon energy ω along the OX axis. Final expressions for Γ_N in the LG SFA and some further details regarding their derivation are given in Appendix A. We have chosen the sign "+" in Eq. (1) (corresponding to the right circular polarization) in the final expressions (A18)–(A21). Of course, the sign "+" and $(n,l) = (2,1)$ mean that both the electric-field vector and the electron rotate counterclockwise. The sign "−" and $(n,l) = (2,-1)$ mean that both the electric-field vector and the electron rotate clockwise. Equation (A21) describes partial ionization rates in these two cases. Equation (A20) concerns a situation when the field and the electron rotate in opposite directions ["+" and $(n,l) = (2,-1)$ or "−" and $(n,l) = (2,1)$]. Analogous expressions for the VG SFA are given in Appendix B.

III. NUMERICAL RESULTS

In this section we present results of our numerical calculations based on Eqs. (A18)–(A21) and (B2), namely, partial ionization rates. Total ionization rates, as a function of the laser frequency and intensity, could also be calculated [see Eq. (15)], but in the present work we are only interested in energy spectra of photoelectrons. (In the 2D case considered here, total ionization rates qualitatively resemble the 3D case; see Figs. 1–4 and 10 from Ref. [8].) In Figs. 1–10 there are the LG SFA energy spectra (solid red lines), which, as we believe, show real physical effects; for example, those discussed in our introduction. Each line is, in fact, a set of points separated by the photon energy, as Eq. (16) shows. For some of the plots, particularly if the line is not a smooth curve, we have added solid circles to underline their discontinuous character. For a comparison we also show the analogous VG SFA energy spectra (dotted blue lines and, at a pinch, open circles). Each of the latter spectra have been normalized to get the same area under both (LG SFA and VG SFA) curves. (Usually the total VG SFA ionization rates are much smaller than the total LG SFA rates.) However, in our humble opinion, the VG SFA spectra might have something in common with the physical reality only in the cases when they qualitatively agree with their LG SFA counterparts. Therefore, in our further discussion, we will concentrate only on the LG results. [The VG results from Figs. 1–10 may be summarized as follows: (i) there is always only a single peak in the ATI envelope; (ii) the peak is for an energy $<U_P$; (iii) the peak moves towards U_P with increasing the laser intensity.] The large number of plots in Figs. 1–10 is connected with our main goal: to investigate photoelectron energy spectra for the total applicability range of the nonrelativisic SFA. (The range is described by two conditions: $z_1 \gg 1$ and $z_f = 2U_P/c^2 \ll 1$.) However, we are aware that for higher laser frequencies and intensities the presented results are beyond current possibility of experimental tests. Thus, we have chosen three intensities and three frequencies for each excited initial state. For the ground state there is only one intensity (Fig. 1), because for the other two intensities the situation looks very similar. The intensities correspond to $z_1 = 50, 250$, and 1250, for which $\gamma = 0.20, 0.089$, and 0.040, respectively. The value of $U_P = z_1E_B/2$ is also shown on each plot by a straight vertical (dashed) line. For each initial state (including the ground one) we have chosen the following set of laser frequencies: $\omega = E_B/5$, $\omega = E_B$, and $\omega = 3E_B$.

In Fig. 1 we present data for the ground state of our 2D atom. There is only a single maximum (or a single peak) for any frequency in either curve. An interesting observation is the following: the LG curves have their maxima closer to the ponderomotive energy than the VG curves. The latter diverge from U_P with increasing the laser frequency towards lower energies in Fig. 1. Nonetheless, both distributions qualitatively look alike. In Fig. 2 we present data for the excited state with $(n,l) = (2,0)$ of our 2D atom in the low-frequency case ($\omega = E_B/5$). Figures 2(a) and 2(b) resemble Fig. 1. However, in Fig. 2(c) we observe two additional small peaks in the ATI envelope: one below and one above U_P. In Fig. 3 we increase the frequency to $\omega = E_B$. Two additional peaks appear already for $z_1 = 50$. Their relative height (with respect to the central

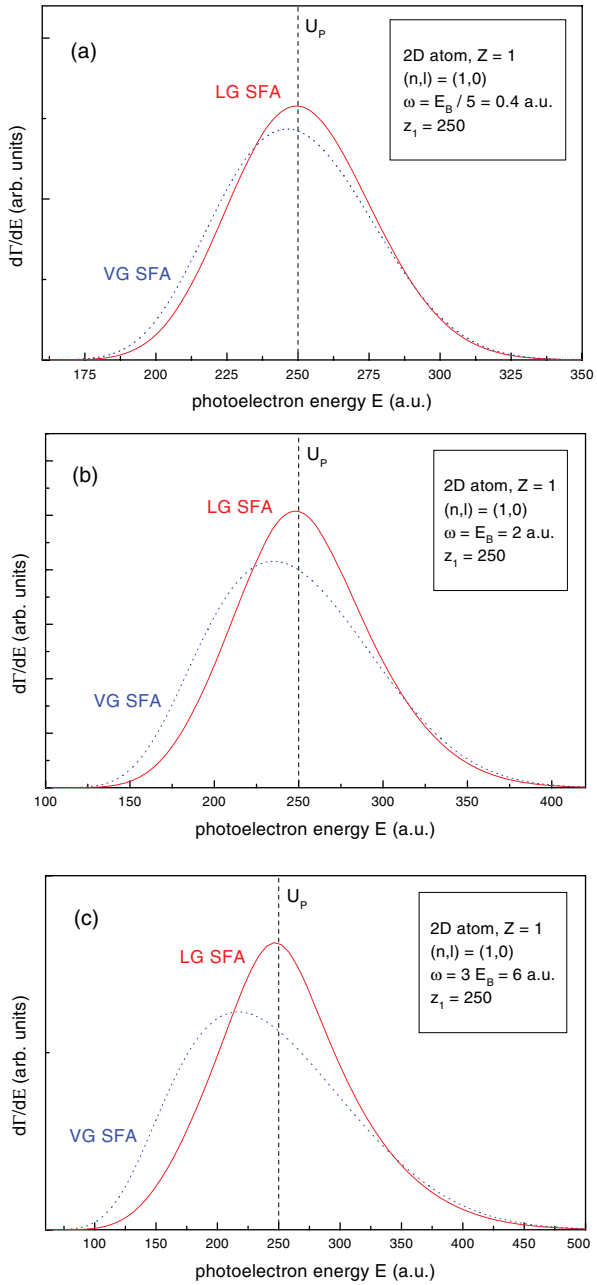

FIG. 1. (Color online) The LG SFA and the VG SFA differential ionization rates of the 2D atom in its ground state [i.e., $(n,l) = (1,0)$] in the (right) circularly polarized plane-wave laser field for three different laser frequencies (one low, one medium, and one high). In each panel [(a), (b), and (c)] the Reiss intensity parameter is the same ($z_1 = 250$), what corresponds to the Keldysh parameter $\gamma = 0.089$. Here the ponderomotive energy is $U_P = 250$ a.u. (see the main text and text frames above for more details).

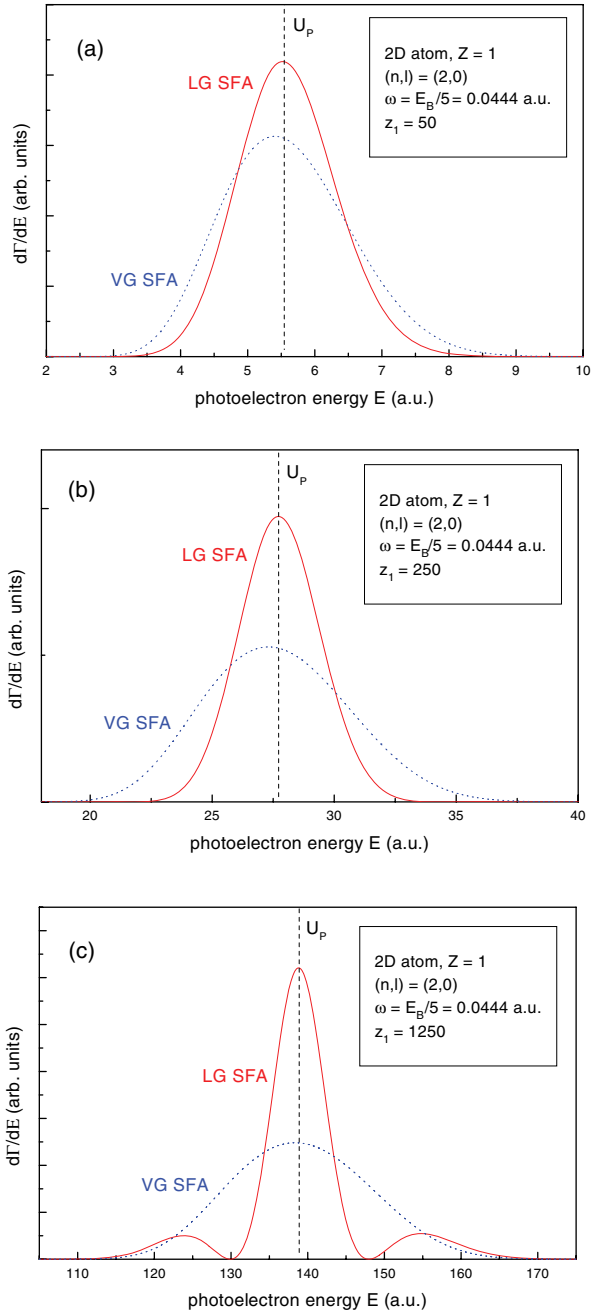

FIG. 2. (Color online) The LG SFA and the VG SFA differential ionization rates of the 2D atom in its first excited state [with $(n,l) = (2,0)$] in the (right) circularly polarized plane-wave laser field for three different laser intensities [corresponding to $z_1 = 50$, 250, and 1250 (or equivalently to $\gamma = 0.20$, 0.089, and 0.040) for panels (a), (b), and (c), respectively]. For these intensities $U_P = 5.56$ a.u., $U_P = 27.8$ a.u., and $U_P = 139$ a.u., respectively. In each panel [(a), (b), and (c)] the laser frequency is $\omega = E_B/5$ (see the main text and text frames above for more details).

peak near U_P) increases with increasing the laser intensity [cf. Figs. 3(a)–3(c)]. Both peaks are asymmetrical regarding their height and width. At the same time the height of the central peak decreases and the peak finally disappears [see Fig. 3(c)]. In Fig. 4 we further increase the frequency to $\omega = 3E_B$. Initially, we have three peaks in the ATI envelope with a very small one near U_P [see Fig. 4(a)]. With increasing the intensity the central peak becomes a local minimum and two other peaks remain, on both sides of the straight vertical line showing U_P [cf. Figs. 4(b) and 4(c)].

In Fig. 5 we present data for the excited state with $(n,l) = (2, -1)$ in the low-frequency case ($\omega = E_B/5$). In Fig. 5(a) there is only one maximum in the ATI envelope at the energy visibly smaller than U_P. It appears that with increasing the

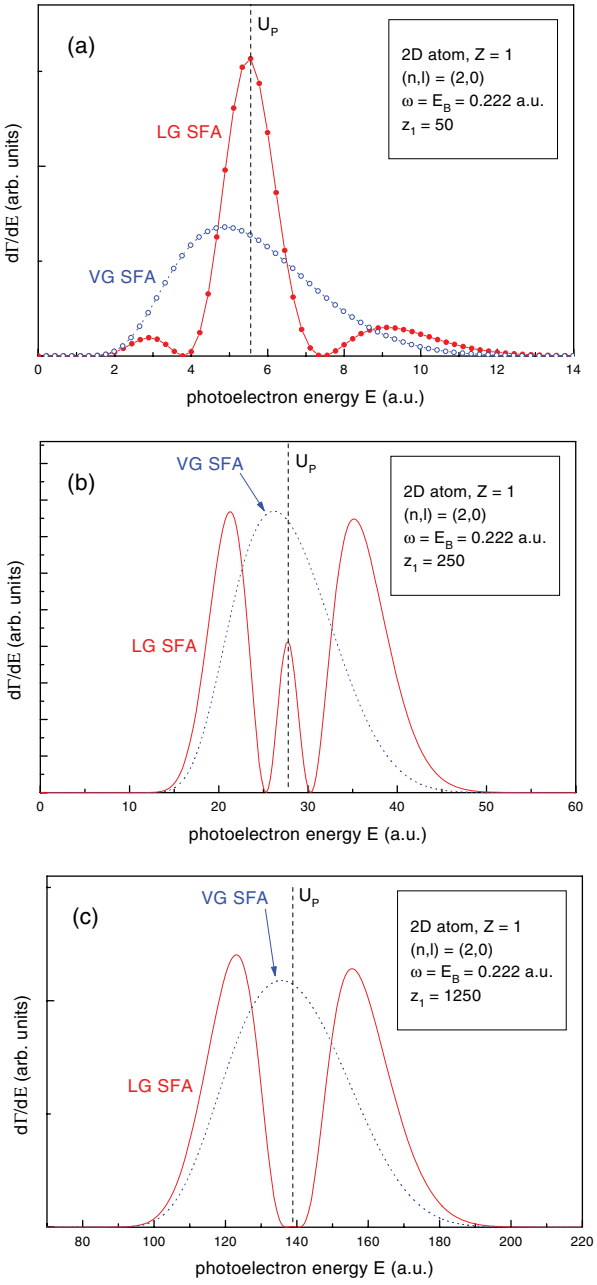

FIG. 3. (Color online) As Fig. 2, but for $\omega = E_B$.

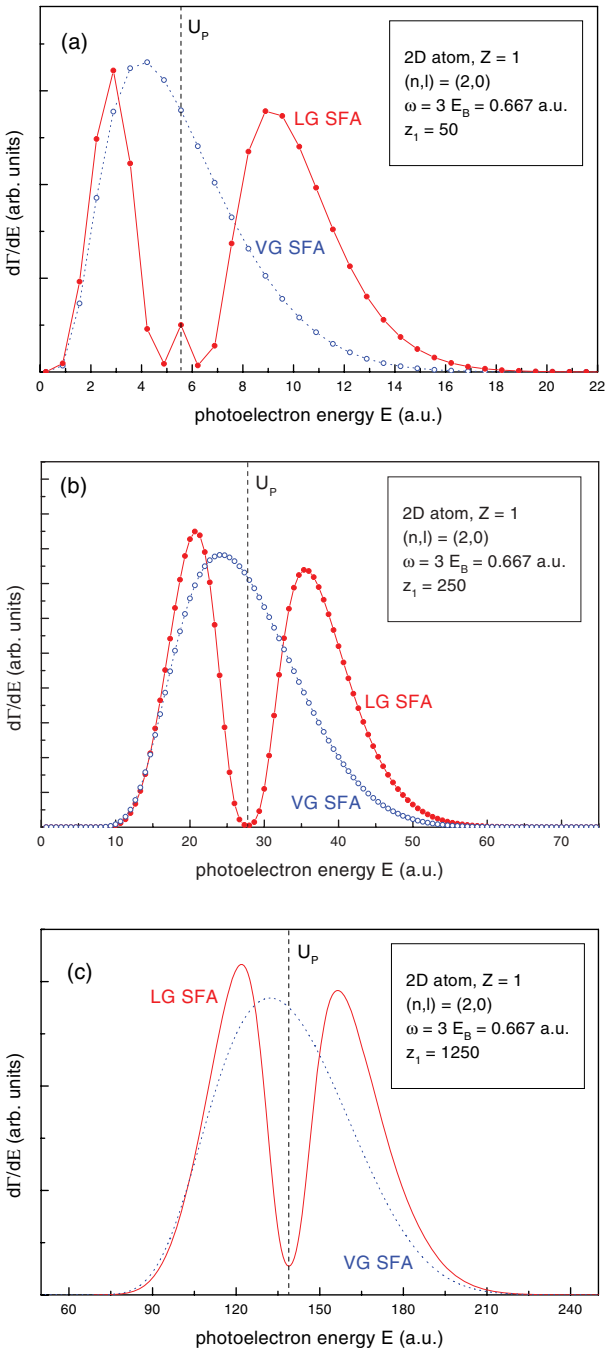

FIG. 4. (Color online) As Fig. 3, but for $\omega = 3E_B$.

intensity another maximum develops at the energy larger than U_P. Initially the peak is very small [see Fig. 5(b)], but becomes clearly visible at $z_1 = 1250$ [see Fig. 5(c)]. The main peak still remains at the energy smaller than U_P. In Fig. 6 we increase the frequency to $\omega = E_B$. Figure 6 qualitatively resembles Fig. 5, but the additional peak (at the energy greater than U_P) is more visible. It is present already at $z_1 = 50$ [see Fig. 6(a)], unlike in Fig. 5(a). What happens if we further increase the frequency to $\omega = 3E_B$? This is shown in Fig. 7. This figure qualitatively resembles Figs. 5 and 6, but the additional peak (at the energy greater than U_P) is yet more visible. As a result, to make the second (smaller) peak as high as possible, one should take the highest frequency and intensity for the $(n,l) = (2, -1)$ initial state. This is exemplified in Fig. 7(c).

Figures 8–10 are analogous to Figs. 5–7, but correspond to the $(n,l) = (2,1)$ initial state. Comparing Fig. 8(a) with Fig. 5(a), Fig. 8(b) with Fig. 5(b), and so on to Fig. 10(c) with Fig. 7(c), we observe nearly mirror-reflection symmetry between the respective curves. The symmetry is, of course, only approximate. For example, the ratio of heights of smaller and larger peaks is greater for the $(n,l) = (2,-1)$ state than for the $(n,l) = (2,1)$ state [cf. Figs. 7(c) and 10(c)].

IV. DISCUSSION AND CONCLUSIONS

We have observed additional peaks at energies different than U_P for most of the photoelectron energy spectra presented

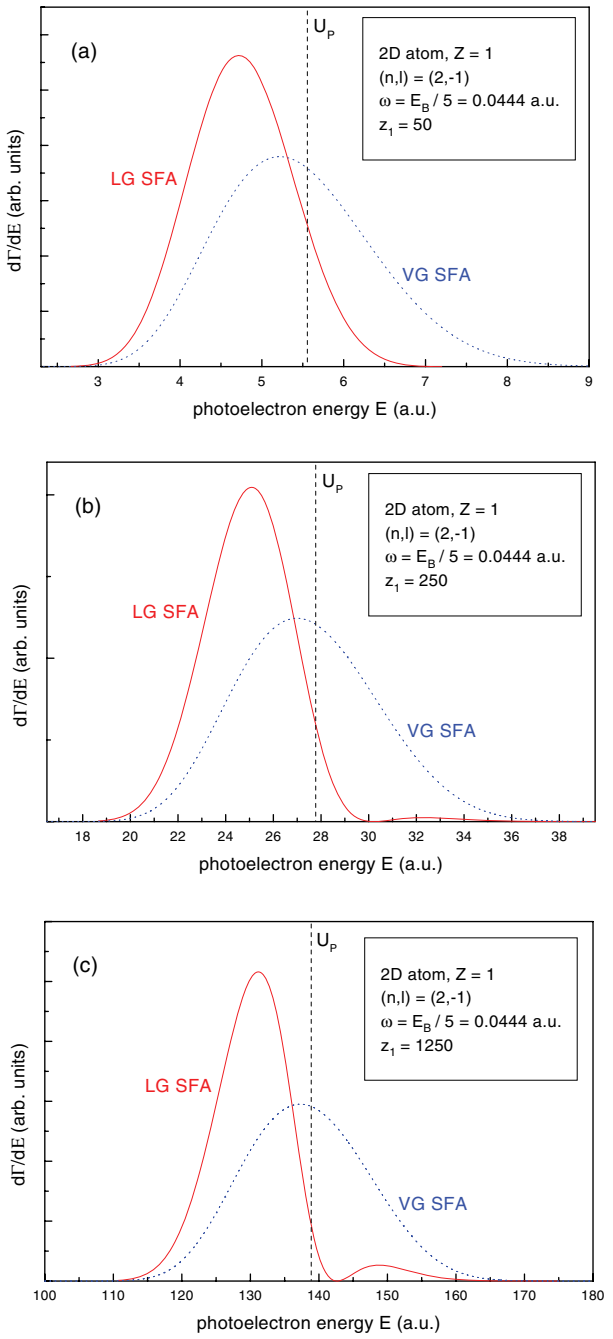

FIG. 5. (Color online) As Fig. 4, but for $(n,l) = (2,-1)$ and $\omega = E_B/5$.

here. In some cases the central, classically expected peak near U_P has disappeared. These phenomena are absent in the VG SFA. Let us compare again probability amplitudes of the ionization in the LG [Eq. (5)] and in the VG [Eq. (B1)]. It is obvious that the phenomena are connected with the preexponential factor in the LG. The factor is time dependent and hangs on the initial-state wave function. We can conjecture, looking at Eqs. (A7)–(A10), that the multi-peak ATI envelope is caused by a non-trivial dependence on $\vec{p}$, either in a radial part [when $(n,l) = (2,0)$, Eq. (A8)] or in an angular part [when $(n,l) = (2,-1)$, Eq. (A9) or $(n,l) = (2,1)$, Eq. (A10)] of the initial-state wave function. As a result, one

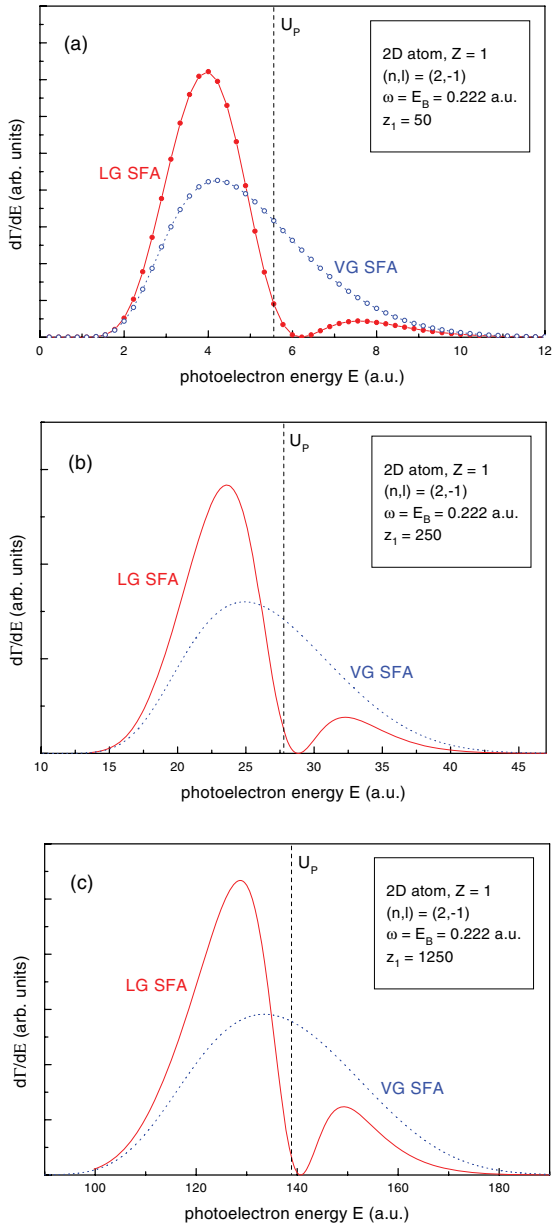

FIG. 6. (Color online) As Fig. 5, but for $\omega = E_B$.

should expect similar phenomena in higher excited (bound) states of the 2D atom, because their wave functions $\tilde{\Phi}_{nl}(\vec{p})$ are yet more complicated.

Some of the bound states (n,l,m) of the 3D atom have their analogs in the shape of the (n,l) states of the 2D atom. The $1s$ (ground) state $(n,l,m) = (1,0,0)$ corresponds to $(n,l) = (1,0)$, the $2s$ state $(n,l,m) = (2,0,0)$ corresponds to $(n,l) = (2,0)$, and the states $2p_\pm$ $(n,l,m) = (2,1,\pm1)$ correspond to $(n,l) = (2,\pm1)$. The state $2p_0$ $(n,l,m) = (2,1,0)$ has no counterpart in two dimensions. Therefore, one should expect a similar multipeak behavior of the ATI envelope in the 3D case in the polarization plane. In fact, we found such behavior for the states $2p_\pm$ in Ref. [17] and for the $2s$ state [23]. Figures 5–10 show generally that when the electron initially rotates against the laser field one should expect a smaller final kinetic energy than for the corotated electrons. Of course, this is true only on average and for the same laser frequency and intensity.

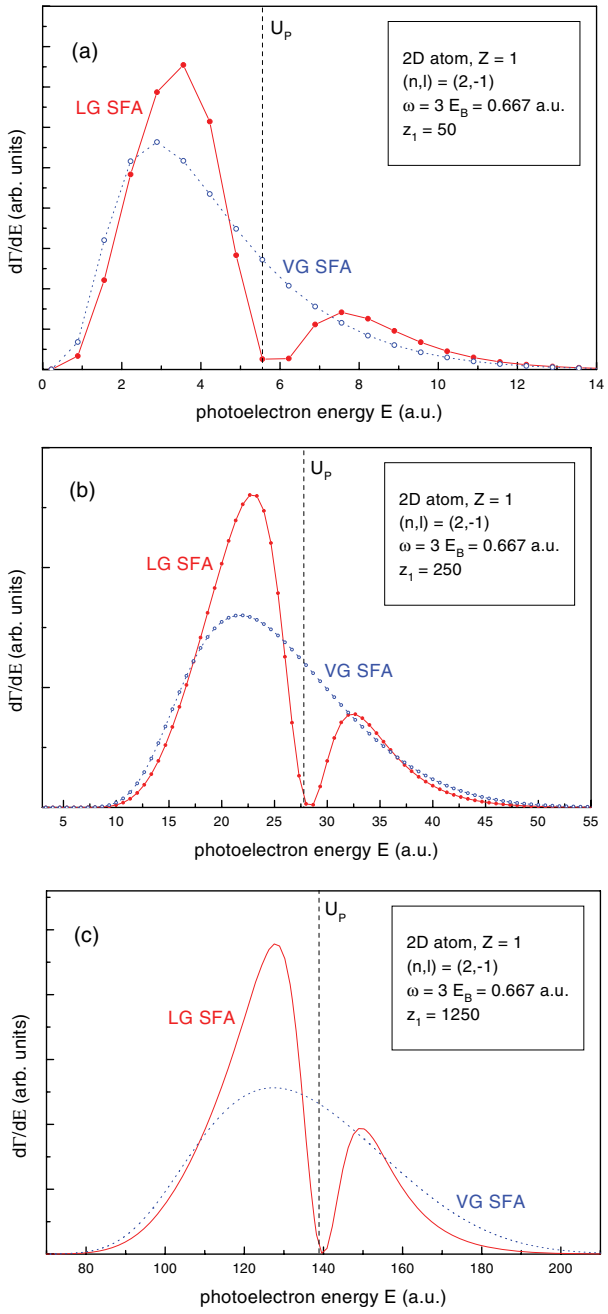

FIG. 7. (Color online) As Fig. 6, but for $\omega = 3E_B$.

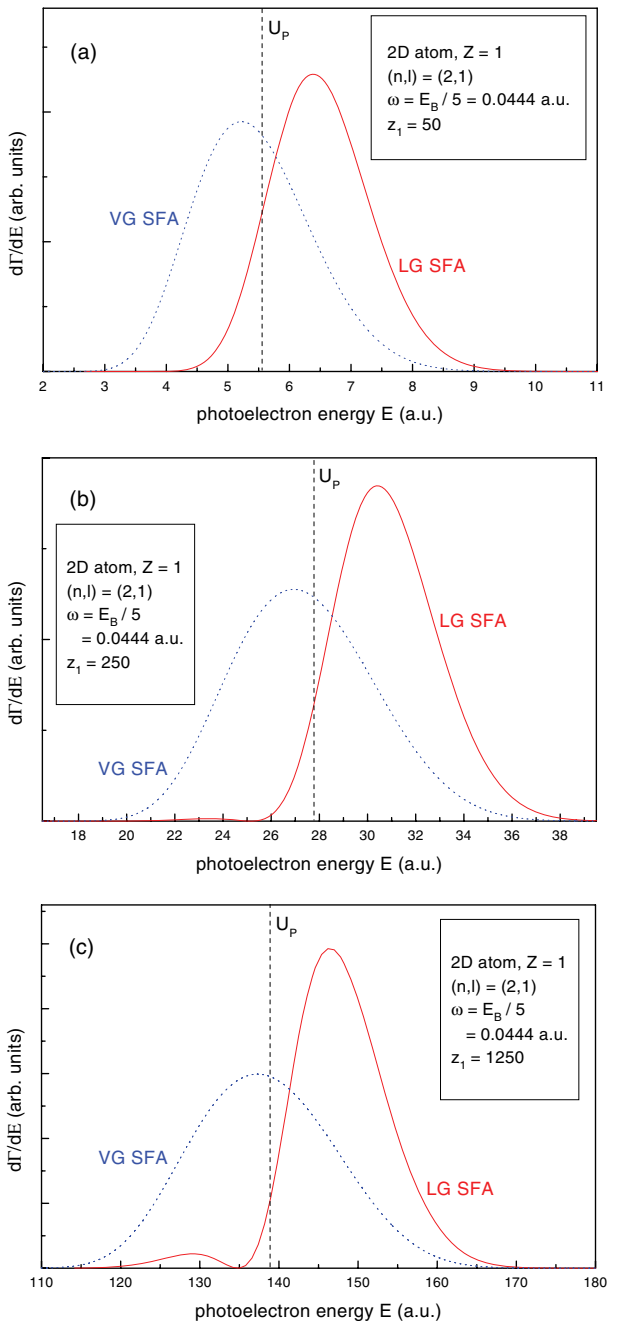

FIG. 8. (Color online) As Fig. 7, but for $(n,l) = (2,1)$ and $\omega = E_B/5$.

Figures 1–4 show that one should expect some intermediate final kinetic energy (only on average) very close to U_P, if the electron initially does not rotate ($l = 0$). On the other hand, vanishing of the central peak (near U_P), and the formation of two other peaks [see, particularly, Figs. 3(b), 3(c), 4(b), and 4(c)] for $(n,l) = (2,0)$, have given us a great surprise. The asymmetry of the ATI spectra (among states with $n = 2$) seems to be understood, if we take into account that the final (Volkov) state is the same in these three cases ($l = -1,0$, and 1). It describes the ionized electron corotating with the laser field. However, further insight into the nature of the observed peaks in the ATI envelope requires, for instance, some kind of a saddle-point analysis (see, for example, Refs. [24–26]). We believe that it is possible, although it may be quite complicated because of the preexponential factor in the ionization amplitude of the LG SFA [Eq. (5)]. In the VG SFA a single saddle point is sufficient to describe well, at the qualitative level, the ATI envelope [23]. We are aware that SFA should be modified to include Coulomb corrections in the final (Volkov) state for lower intensities and shorter pulses [24]. On the other hand, in the Landau-Dykhne approach [27,28], the effect of the initial-state wave function on the photoelectron energy spectra is completely neglected. One can show that for superstrong laser fields effects predicted by the LG SFA appear for lower intensities than relativistic effects in the Landau-Dykhne approach. Furthermore, unlike the latter, the

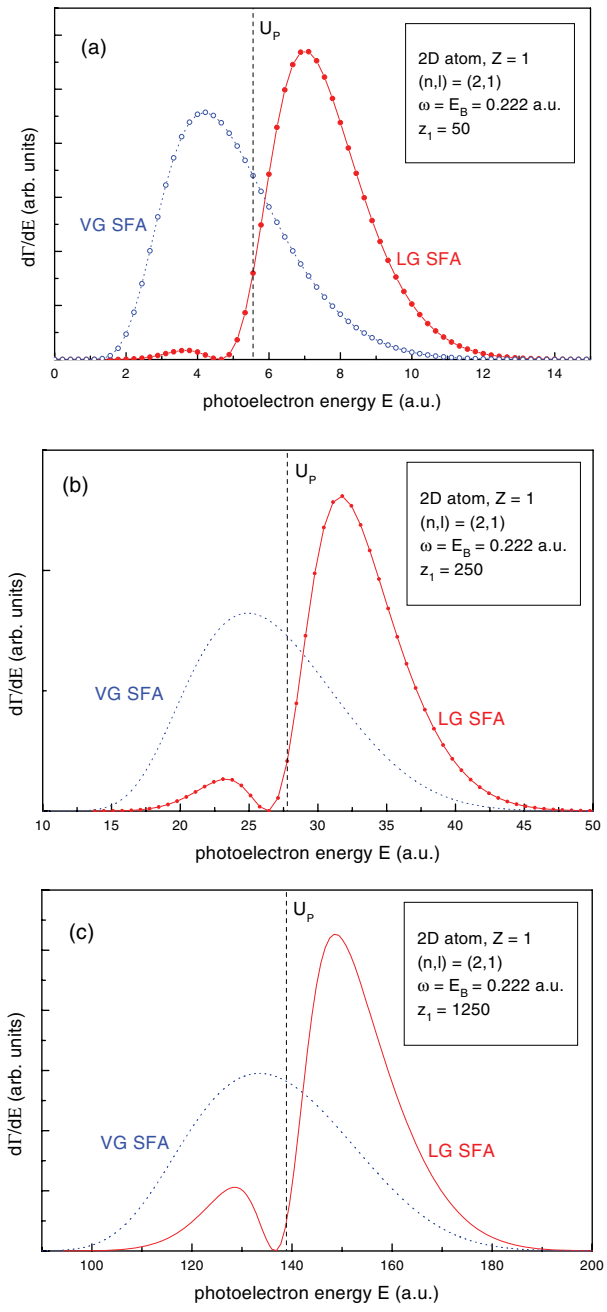

FIG. 9. (Color online) As Fig. 8, but for $\omega = E_B$.

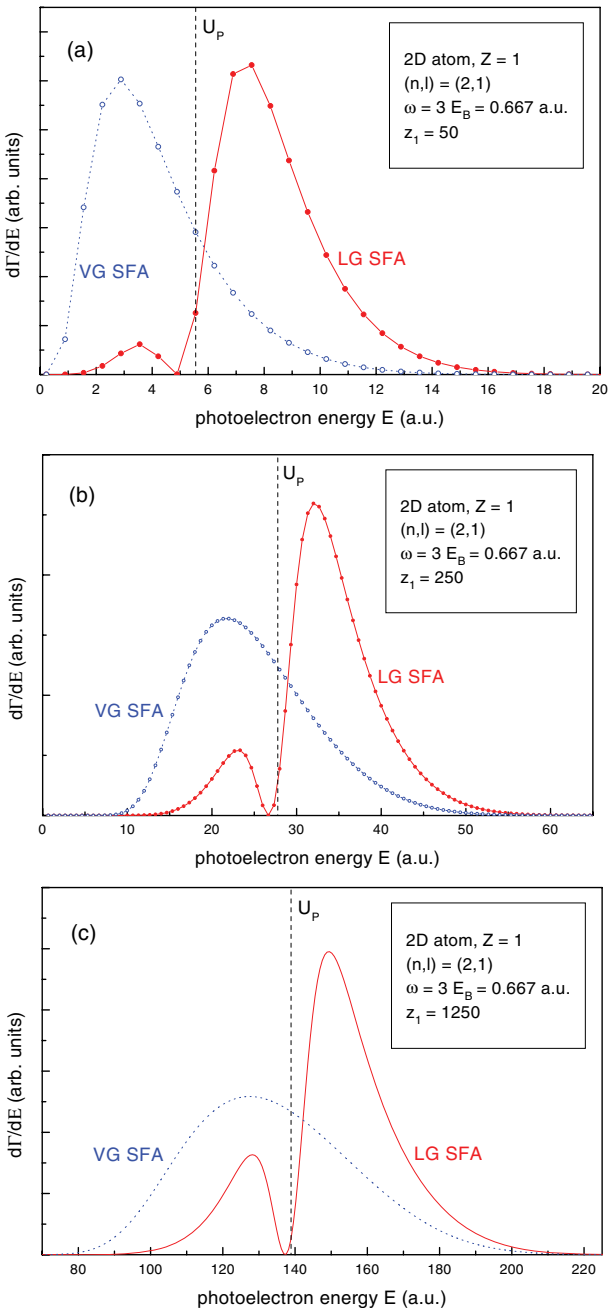

FIG. 10. (Color online) As Fig. 9, but for $\omega = 3E_B$.

LG SFA shows the multipeak ATI envelope in a full solid angle (see Figs. 12 and 13 in Ref. [8]).

We note that different total ionization rates were predicted for a nonadiabatic tunneling in the CP laser field for the $4p$ (excited) state of krypton [26]. There is a slight relative shift in the single-peak ATI envelopes between p_- and p_+ initial states for the parameter $z_1 \approx 2.2$ [26]. The direction of this shift is in agreement with relative shifts of our main peaks [cf. Figs. 5(a) and 8(a): the low-frequency case, but we have $z_1 = 50$ here and $n = 2$ instead of $n = 4$ (principal quantum numbers)]. We also note that for the CP field and the $2p$ hydrogen atom (in three different initial states with $m = -1, 0,$ and 1) by a 20-cycle sine-square laser pulse (with $\omega = 2E_B$) the ionization depends on the azimuthal quantum number m in Ref. [29]. In this *ab initio* calculation the asymmetry between the initial states $(2,1,-1)$ and $(2,1,1)$ also appeared in the photoelectron energy spectra after switching off the laser field (thus these results are gauge invariant). The highest peak field, applied therein, corresponded to $z_1 \approx 72$ [cf. Figs. 11 and 13 in Ref. [29]].

In conclusion, the 2D LG SFA (nonrelativistic) photoelectron energy spectra usually show the multipeak ATI envelope for CP laser fields. This is probably a typical situation for most of the excited states (with the principal quantum number $n > 1$), although we have verified this statement only for $n = 2$. A similar existence of a multipeak envelope was found previously in the 3D case (both in the full solid angle [8] and in the polarization plane [17,23]). On the whole, we connect

this phenomena with a nontrivial functional dependence (on $\vec{r}$ or $\vec{p}$) of the initial-state wave function (respectively, in the spatial or the momentum representation). The 2D wave functions (n,l) resemble some of the 3D wave functions (n,l,m) in the polarization plane. Therefore, one can expect similar phenomena in 2D and in 3D. Only LG SFA results show the multipeak ATI envelope for CP laser fields, because (in fact) these results are gauge invariant. In the ATI spectrum one can see only this part of the energy absorbed from the field, which is connected with a drift of the ionized electron. The rest of the energy is connected with the circular motion (with frequency ω, and radius $\alpha_0 = F/\omega^2$) in phase with the laser field. (If the field is switched off slow enough, as for long laser pulses, one does not observe finally any effect in the energy spectrum.) For the initial state $(n,l) = (2,-1)$ the main peak exists below U_P, because some amount of the energy absorbed from the laser field should be taken to make the ionized electron rotate in the direction opposite than before. For the initial state $(n,l) = (2,1)$ the main peak exists above U_P, because roughly the same amount of energy need not be taken from the field because the ionized electron initially already rotates in the same direction as the laser field. For the initial state $(n,l) = (2,0)$ the main peak exists near U_P, if the field intensity is not too high. If the latter increases, two additional peaks arise, but in such a way that the mean energy is still very close to U_P. Although differences in the angular momentum (among states with $n = 2$ and $l = -1,0$, and 1) are small, intense laser fields create large differences in shapes of ATI envelopes. [Note that initial kinetic energy probability distributions are identical for $(n,l) = (2,-1)$ and $(n,l) = (2,1)$, but are quite different for $(n,l) = (2,0)$. $\tilde{\Phi}_{20}(\vec{p})$ has an additional node at $p = k = 2Z/3$, which does not exist for other initial states considered here.] Similar high sensitivity to initial quantum number m in 3D was observed in Refs. [26,29]. A further detailed explanation of positions and widths of peaks in ATI envelopes requires an analysis, which is beyond the scope of the present work. Perhaps saddle-point or classical-trajectory Monte Carlo methods could be useful here. We would like to get some more physical insight into the process studied here by applying one of these methods in the future. However, there is no room for doubt about the very existence of the phenomena shown in Figs. 1–10. In our humble opinion, the results presented in this work give another exemplary answer to the question formulated by Bauer *et al.* in Ref. [10]: "Which gauge is better suited for above-threshold ionization of atoms and molecules as well as nonsequential double ionization?". Presented results are valid in the limit of an infinite flat pulse (its spectral width is zero). It is also of interest studying photoelectron energy spectra (resulting from the SFA) for a finite pulse in the adiabatic approximation. We plan to test the present 2D model for both SFA gauges by exact (numerical) solutions of the time-dependent Schrödinger equation [22], regarding both total ionization rates and photoelectron energy spectra.

ACKNOWLEDGMENTS

The present paper has been supported by the University of Łódź. The author is indebted to the anonymous referee for useful remarks.

APPENDIX A

In this work we use (in the spatial representation) the following initial-state wave functions, which are solutions to Eq. (7). Introducing $\beta_n = 2Z/(n - 1/2)$, for $n = 1$ and 2, one obtains $\Phi_{nl}(r,\phi')$—the first two bound states [r and ϕ' denote the polar coordinates of $\vec{r} = (x,y) = (r\ \cos\ \phi', r\ \sin\ \phi')$] [21]:

$$\Phi_{10}(r,\phi') = \frac{\beta_1}{\sqrt{2\pi}} \exp(-\beta_1 r/2), \tag{A1}$$

$$\Phi_{20}(r,\phi') = \frac{\beta_2}{\sqrt{6\pi}}(1 - \beta_2 r)\exp(-\beta_2 r/2), \tag{A2}$$

$$\Phi_{2,-1}(r,\phi') = \frac{\beta_2^2}{\sqrt{12\pi}} r\ \exp(-\beta_2 r/2)\exp(-i\phi'), \tag{A3}$$

$$\Phi_{2,+1}(r,\phi') = \frac{\beta_2^2}{\sqrt{12\pi}} r\ \exp(-\beta_2 r/2)\exp(i\phi'). \tag{A4}$$

The above wave functions obey the normalization condition

$$\int |\Phi_{nl}(r,\phi')|^2 r\, dr\, d\phi' = 1. \tag{A5}$$

They can be Fourier transformed in the 2D space

$$\tilde{\Phi}_{nl}(\vec{p}) = \int \frac{r\, dr\, d\phi'}{2\pi} \Phi_{nl}(\vec{r}) \exp(-i\,\vec{p}\vec{r}) \tag{A6}$$

by integrations first over r and then (with the help of the residue theorem) over ϕ'. To simplify further equations let us introduce two new notations: $\beta = \beta_1/2 = 2Z$ and $k = \beta_2/2 = 2Z/3$ (here k is a real number and should not be confused with the index of previous summations). Let us note that $E_B = \beta^2/2 = 2Z^2$ for $(n,l) = (1,0)$ and $E_B = k^2/2 = 2Z^2/9$ for $(n,l) = (2,-1)$, $(n,l) = (2,0)$, and $(n,l) = (2,1)$. If p and ϕ denote polar coordinates of the momentum $\vec{p}$, one obtains the following momentum-space wave functions for the ground state:

$$\tilde{\Phi}_{10}(p,\phi) = \sqrt{\frac{2}{\pi}} \frac{\beta^2}{(p^2 + \beta^2)^{3/2}}, \tag{A7}$$

and for the first excited state

$$\tilde{\Phi}_{20}(p,\phi) = \sqrt{\frac{6}{\pi}} \frac{k^2(p^2 - k^2)}{(p^2 + k^2)^{5/2}}, \tag{A8}$$

$$\tilde{\Phi}_{2,-1}(p,\phi) = \sqrt{\frac{12}{\pi}} \frac{k^3 p}{(p^2 + k^2)^{5/2}} \frac{\exp(-i\phi)}{i}, \tag{A9}$$

$$\tilde{\Phi}_{2,+1}(p,\phi) = \sqrt{\frac{12}{\pi}} \frac{k^3 p}{(p^2 + k^2)^{5/2}} \frac{\exp(i\phi)}{i}. \tag{A10}$$

The above momentum-space wave functions obey the normalization condition

$$\int |\tilde{\Phi}_{nl}(p,\phi)|^2 p\, dp\, d\phi = 1. \tag{A11}$$

The Fourier coefficients $A_k(\vec{p})$ from Eq. (9) are calculated as follows. Multiplying both sides of Eq. (9) by $\exp[-im(\omega t + \varphi_0 \mp \phi)]$ and integrating both sides upon time from 0 to $T = 2\pi/\omega$, utilizing the relation (m and s are integer numbers)

$$\int_0^{2\pi} dx\ \exp(isx) = 2\pi\delta_{s0}, \tag{A12}$$

one obtains for $(n,l) = (1,0)$ the formula

$$A_m(\vec{p}) = \frac{\beta^2}{\sqrt{2\pi^3(p^2+\beta^2+2z\omega)}} \int_0^\pi \frac{dx\ \cos mx}{\sqrt{1+q\ \cos x}}, \tag{A13}$$

where $q = \sqrt{8z\omega}p/(p^2+\beta^2+2z\omega)$ and $0 < q < 1$. For $(n,l) = (2,0)$ one obtains the following analogous Fourier coefficient:

$$B_m(\vec{p}) = \frac{\sqrt{6}k^2}{\pi^{3/2}(p^2+k^2+2z\omega)^{3/2}} \times \int_0^\pi \frac{dx(a+b\ \cos x)\cos mx}{(1+q'\ \cos x)^{3/2}}, \tag{A14}$$

where $q' = \sqrt{8z\omega}p/(p^2+k^2+2z\omega)$ (and $0 < q' < 1$), $a = p^2-k^2+2z\omega$, and $b = \sqrt{8z\omega}p$. For the states $(n,l) = (2,-1)$ and $(n,l) = (2,1)$ all calculations, leading to the final result, are more laborious. In this case we make the following Fourier expansion:

$$[p^2+k^2+2z\omega+\sqrt{8z\omega}p\ \cos(\omega t+\varphi_0\mp\phi)]^{-3/2} = \sum_{k=-\infty}^{\infty} C_k(\vec{p})\exp[ik(\omega t+\varphi_0\mp\phi)]. \tag{A15}$$

Multiplying both sides of Eq. (A15) by $\exp[-im(\omega t+\varphi_0\mp\phi)]$ and integrating both sides upon time from 0 to T, utilizing the relation (A12), one obtains

$$C_m(\vec{p}) = \frac{1}{\pi(p^2+k^2+2z\omega)^{3/2}} \int_0^\pi \frac{dx\ \cos mx}{(1+q'\ \cos x)^{3/2}}. \tag{A16}$$

Let us notice that the left-hand side (LHS) of Eq. (A15) is only a denominator of the expression from the LHS of Eq. (9) for the states $(n,l) = (2,-1)$ and $(n,l) = (2,1)$.

The crux of the matter, in the calculation of ionization rates for these states, lies in the fact that the LHS of Eq. (9) also contains factors proportional to the length $|\vec{\pi}(t)|$ and the phase factor $\exp[\pm i\theta(t)]$ of the time-dependent kinetic momentum vector $\vec{\pi}(t) = \vec{p}+\vec{A}(t)/c$, where

$$|\vec{\pi}(t)| = \sqrt{\vec{\pi}(t)^2} = \sqrt{p^2+2z\omega+\sqrt{8z\omega}p\ \cos(\omega t+\varphi_0\mp\phi)} \tag{A17}$$

and $\vec{\pi}(t) = \hat{x}|\pi(t)|\cos\theta(t)+\hat{y}|\pi(t)|\sin\theta(t)$. To calculate $(S-1)_{fi}^{\mathrm{LGSFA}}$ we have to increase or decrease (±1) indices of some summations in Eq. (13). This is possible, because both summations extend from $-\infty$ to $+\infty$. Finally we get the following expressions for partial ionization rates $\Gamma_N^{(n,l)}$:

$$\Gamma_N^{(1,0)} = \left[2\pi\sum_{j=-\infty}^{\infty}(-1)^j A_j(p_N)J_{N+j}\left(\sqrt{\frac{2z}{\omega}}p_N\right)\right]^2, \tag{A18}$$

$$\Gamma_N^{(2,0)} = \left[2\pi\sum_{j=-\infty}^{\infty}(-1)^j B_j(p_N)J_{N+j}\left(\sqrt{\frac{2z}{\omega}}p_N\right)\right]^2, \tag{A19}$$

$$\Gamma_N^{(2,-1)} = \frac{2^{10}Z^6\pi}{3^5}\left\{\sum_{j=-\infty}^{\infty}(-1)^j C_j(p_N)\left[\frac{p_N}{2}J_{N+j}\left(\sqrt{\frac{2z}{\omega}}p_N\right) - \sqrt{\frac{z\omega}{2}}J_{N+j-1}\left(\sqrt{\frac{2z}{\omega}}p_N\right)\right]\right\}^2, \tag{A20}$$

$$\Gamma_N^{(2,1)} = \frac{2^{10}Z^6\pi}{3^5}\left\{\sum_{j=-\infty}^{\infty}(-1)^j C_j(p_N)\left[\frac{p_N}{2}J_{N+j}\left(\sqrt{\frac{2z}{\omega}}p_N\right) - \sqrt{\frac{z\omega}{2}}J_{N+j+1}\left(\sqrt{\frac{2z}{\omega}}p_N\right)\right]\right\}^2. \tag{A21}$$

In the LHS of Eqs. (A13), (A14), and (A16) the Fourier coefficients depend on $\vec{p}$. However, the integration upon time leading to the right-hand side of these equations removes their ϕ dependence. So, finally, they become functions of p only. The integrands in Eqs. (A13), (A14), and (A16) are rapidly oscillating functions of x for $|m| \gg 1$. It is possible to calculate these integrals analytically, expressing them by a hypergeometric function. However, in this work we have chosen another method. The integrals are calculated by a special method for rapidly varying integrands, namely, by some extension of the Filon method [30]. To increase accuracy in the respective FORTRAN code we have used numbers with a precision of approximately 33 decimal digits (the type of REAL 16) and about 1000 points dividing the interval of integration $[0,\pi]$.

APPENDIX B

In the VG SFA one starts from the ionization probability amplitude [7,8,14]

$$(S-1)_{fi}^{\mathrm{VGSFA}} = i\int_{-\infty}^{\infty} dt\tilde{\Phi}_i(\vec{p})\left(\frac{1}{2}\vec{p}^2+E_B\right) \times \exp\left[\frac{i}{2}\int_{-\infty}^{t}\left(\vec{p}+\frac{1}{c}\vec{A}(\tau)\right)^2 d\tau + iE_B t\right]. \tag{B1}$$

Let us note that $(S-1)_{fi}^{\mathrm{LGSFA}}$ [Eq. (5)] is a function of the kinetic momentum $\vec{\pi}(t) = \vec{p}+\vec{A}(t)/c$ of the ionized electron only. $(S-1)_{fi}^{\mathrm{VGSFA}}$ does not have this property. It depends partly on the canonical momentum $\vec{p}$ and partly on $\vec{\pi}(t)$. The lack of time dependence in the first two factors in the above integrand makes all the calculations much easier. Instead of two Fourier expansions for the LG SFA, now only a single one [namely, that from Eq. (11)] is sufficient to calculate the ionization rate. Applying analogous steps we finally obtain

$$\Gamma_N'^{(n,l)} = \left[2\pi\left(\frac{p_N^2}{2}+E_B\right)|\tilde{\Phi}_{nl}(p_N)|J_N\left(\sqrt{\frac{2z}{\omega}}p_N\right)\right]^2, \tag{B2}$$

where we put the prime on Γ to distinguish the VG SFA partial ionization rate from its LG SFA counterpart. In Eq. (B2) $E_B = 2Z^2$ for $(n,l) = (1,0)$ and $E_B = 2Z^2/9$ for $(n,l) = (2,-1)$, $(n,l) = (2,0)$, and $(n,l) = (2,1)$. In particular, it follows from Eqs. (B2), (A9), and (A10) that $\Gamma_N'^{(2,-1)} = \Gamma_N'^{(2,1)}$. Moreover, let us consider a more general initial state (a quantum-mechanical

superposition) given by

$$\Phi_{\text{initial}} = \alpha\Phi_{2,-1} + \beta\Phi_{2,1}, \tag{B3}$$

where α and β are arbitrary complex numbers such that $|\alpha|^2 + |\beta|^2 = 1$. Substituting Eq. (B3) into Eq. (B1) one gets the same result (B2) [with $(n,l) = (2,\pm 1)$] for Φ_{initial} (regardless of α and β). This is the result of the integration upon ϕ [we are reminded that $\vec{p} = (p_x, p_y) = (p\cos\phi, p\sin\phi)$] and Eq. (A12), which causes those terms containing the product $\tilde{\Phi}^*_{2,1}\tilde{\Phi}_{2,-1}$ or its complex conjugate $\tilde{\Phi}_{2,1}\tilde{\Phi}^*_{2,-1}$ to not contribute to the final expression.

APPENDIX C

Let us assume that the laser field, which is adiabatically turned on and off at asymptotic times ($t \to \pm\infty$), changes somehow in time. (In the S-matrix theory a monochromatic laser field of constant amplitude is considered, but here this condition is superfluous.) The laser field can be described by the vector potential $\vec{A}$ (in the Coulomb gauge, in the dipole approximation), for which one usually assumes that

$$\lim_{t\to\pm\infty} \vec{A}(t) = \vec{0}. \tag{C1}$$

The magnetic-field component of the laser field is zero and the electric-field component is given by

$$\vec{F}(t) = -\frac{1}{c}\frac{\partial\vec{A}}{\partial t}. \tag{C2}$$

(We use cgs units throughout Appendix C.) Let us note [see Eq. (C2)] that the condition (C1) is stronger than the condition $\lim_{t\to\pm\infty} \vec{F}(t) = \vec{0}$. The one-electron atom or ion in the laser field is described by the following Hamiltonian:

$$H = H_A + H_I \equiv \frac{\hat{\vec{p}}^2}{2m} + V(\vec{r}) + H_I, \tag{C3}$$

where H_A is the atomic Hamiltonian, and the interaction Hamiltonian is given either in the $\vec{p}\vec{A}$ (or VG) form:

$$H_I^{pA} = \frac{-e}{mc}\vec{A}(t)\hat{\vec{p}} + \frac{e^2}{2mc^2}\vec{A}(t)^2 \tag{C4}$$

($e < 0$ is the charge of an electron and $\hat{\vec{p}} = -i\hbar\vec{\nabla}$) or in the $\vec{d}\vec{E}$ (or LG) form:

$$H_I^{dE} = -e\vec{r}\vec{F}(t). \tag{C5}$$

Using the usual rules of quantum mechanics for both wave functions and operators ($\Psi' = \hat{U}\Psi$, $\hat{O}' = \hat{U}\hat{O}\hat{U}^{-1}$), the time-dependent Schrödinger equation (TDSE), for the atom in the laser field, can be transformed from either form to the other one by a certain unitary transformation. It is very well known that within the dipole approximation of the laser field the above-mentioned two descriptions are equivalent. Let $\Psi(\vec{r},t)$ be the exact solution of the TDSE with the Hamiltonian (C3) in either form, and $\Phi(\vec{r},t)$ be the exact solution of the TDSE with Hamiltonian H_A. If the subscripts i, f denote initial and final states, one can define two equivalent forms of the exact S matrix:

$$S_{fi} = \lim_{t\to+\infty}(\Phi_f, \Psi_i^{(+)}), \quad \text{where} \quad \lim_{t\to-\infty}\Psi_i^{(+)} = \Phi_i, \tag{C6}$$

$$S_{fi} = \lim_{t\to-\infty}(\Psi_f^{(-)}, \Phi_i), \quad \text{where} \quad \lim_{t\to+\infty}\Psi_f^{(-)} = \Phi_f, \tag{C7}$$

which are called the direct time form and the reversed time form, respectively (the round brackets denote the overlap of two wave functions). We will use the form (C7) here. In this case, making use of the boundary condition for $t \to +\infty$ [the second of Eqs. (C7)], one obtains

$$\begin{aligned}(S-1)_{fi} = S_{fi} - \delta_{fi} &= \lim_{t\to-\infty}(\Psi_f^{(-)},\Phi_i) - \lim_{t\to+\infty}(\Psi_f^{(-)},\Phi_i) = \int_{\infty}^{-\infty} dt\frac{\partial}{\partial t}(\Psi_f^{(-)},\Phi_i)\\ &= -\int_{-\infty}^{\infty} dt\left(\frac{\partial}{\partial t}\Psi_f^{(-)},\Phi_i\right) - \int_{-\infty}^{\infty} dt\left(\Psi_f^{(-)},\frac{\partial}{\partial t}\Phi_i\right) = -\int_{-\infty}^{\infty} dt\left(\frac{1}{i\hbar}(H_A+H_I)\Psi_f^{(-)},\Phi_i\right) - \int_{-\infty}^{\infty} dt\left(\Psi_f^{(-)},\frac{1}{i\hbar}H_A\Phi_i\right)\\ &= -\frac{i}{\hbar}\int_{-\infty}^{\infty} dt(\Psi_f^{(-)}, H_I\Phi_i),\end{aligned} \tag{C8}$$

where the hermiticity of H_A and H_I has been used. The crucial point of this derivation is the following observation: only in the LG equations (C6) and (C7) are there true probability amplitudes of the ionization (or detachment), if the wave functions Φ_f and Φ_i denote the "textbook" [for example Coulomb, if $V(\vec{r}) = -Z/r$] wave functions without any additional phase factors. The reason is as follows. The asymptotic reference states should be eigenstates of the gauge-invariant energy operator in the absence of the laser field. One can show (see the Appendix in Ref. [16]) that this implies that only in the LG do these asymptotic reference states have the form of "textbook" wave functions Φ_f or Φ_i. To get the probability amplitude of the ionization in the VG, first one has to transform these wave functions to this gauge according to the above-mentioned quantum-mechanical rule

$$\Psi^{pA}(\vec{r},t) = \hat{U}(\vec{r},t)\Psi^{dE}(\vec{r},t), \tag{C9}$$

where $\hat{U}(\vec{r},t) = \exp[(ie/\hbar c)\vec{r}\vec{A}(t)]$ is the unitary operator which assures gauge invariance. This exponential operator transforms the TDSE with the Hamiltonian (C3) (both wave functions and operators) from the LG to the VG. Therefore, one has to multiply the wave function $\Psi^{pA}(\vec{r},t)$ by the operator $\hat{U}^+(\vec{r},t) = \exp[(-ie/\hbar c)\vec{r}\vec{A}(t)]$ before projecting on an eigenstate of the atomic Hamiltonian. In such a way one

obtains the overlap, which is gauge invariant and can be treated as an instantaneous probability amplitude of ionization (or detachment). This is equivalent to multiplying of the wave function $\Psi^{dE}(\vec{r},t)$ by the operator $\hat{U}(\vec{r},t)$, when working in the VG. For sufficiently weak electric fields described by $\vec{A}(t)$ one can sometimes approach $\hat{U}(\vec{r},t)$ by unity, but for strong fields setting $\hat{U}(\vec{r},t) \cong 1$ is certainly not justified. For example, for the $H(1s)$ atom, if $|\vec{r}| \cong 1$a.u. the exponent in Eq. (C9) is of the order of $i\sqrt{z_1}$. The counterparts of Eqs. (C6) and (C7) in the VG are the following equations:

$$S_{fi} = \lim_{t\to+\infty}\left(\hat{U}\Phi_f,\Psi_i^{(+)pA}\right) = \lim_{t\to+\infty}\left(\Phi_f,\hat{U}^+\Psi_i^{(+)pA}\right), \quad \text{where} \quad \lim_{t\to-\infty}\Psi_i^{(+)pA} = \hat{U}\Phi_i, \tag{C10}$$

$$S_{fi} = \lim_{t\to-\infty}\left(\Psi_f^{(-)pA},\hat{U}\Phi_i\right) = \lim_{t\to-\infty}\left(\hat{U}^+\Psi_f^{(-)pA},\Phi_i\right), \quad \text{where} \quad \lim_{t\to+\infty}\Psi_f^{(-)pA} = \hat{U}\Phi_f. \tag{C11}$$

To obtain a correct and exact result in the VG (for the reversed time S matrix) we have to start from Eqs. (C11).

$$\begin{aligned}(S-1)_{fi} = S_{fi} - \delta_{fi} &= \lim_{t\to-\infty}\left(\Psi_f^{(-)pA},\hat{U}\Phi_i\right) - \lim_{t\to+\infty}\left(\Psi_f^{(-)pA},\hat{U}\Phi_i\right) = \int_{\infty}^{-\infty} dt\,\frac{\partial}{\partial t}\left(\hat{U}^+\Psi_f^{(-)pA},\Phi_i\right)\\ &= -\int_{-\infty}^{\infty} dt\left(\frac{\partial\hat{U}^+}{\partial t}\Psi_f^{(-)pA},\Phi_i\right) - \int_{-\infty}^{\infty} dt\left(\hat{U}^+\frac{\partial\Psi_f^{(-)pA}}{\partial t},\Phi_i\right) - \int_{-\infty}^{\infty} dt\left(\hat{U}^+\Psi_f^{(-)pA},\frac{\partial\Phi_i}{\partial t}\right)\\ &= -\int_{-\infty}^{\infty} dt\left(\frac{1}{i\hbar}H_I^{dE}\hat{U}^+\Psi_f^{(-)pA},\Phi_i\right) - \int_{-\infty}^{\infty} dt\left(\hat{U}^+\frac{1}{i\hbar}\left(H_A+H_I^{pA}\right)\Psi_f^{(-)pA},\Phi_i\right) - \int_{-\infty}^{\infty} dt\left(\hat{U}^+\Psi_f^{(-)pA},\frac{1}{i\hbar}H_A\Phi_i\right).\end{aligned} \tag{C12}$$

Using Eqs. (C2), (C5) and the hermiticity of H_A, we can add the last three integrals in Eq. (C12) and obtain

$$(S-1)_{fi} = \frac{1}{i\hbar}\int_{-\infty}^{\infty} dt\left(\left(H_I^{dE}\hat{U}^+ + [\hat{U}^+,H_A] + \hat{U}^+H_I^{pA}\right)\Psi_f^{(-)pA},\Phi_i\right). \tag{C13}$$

The calculation of a commutator in the above equation is elementary and gives

$$[\hat{U}^+,H_A] = -\hat{U}^+H_I^{pA}. \tag{C14}$$

Then, after substitution of Eq. (C14) into Eq. (C13), the Hamiltonian H_I^{pA} disappears from the S-matrix element in spite of making calculations in the VG. Finally, because H_I^{dE} is a Hermitian operator, the exact probability amplitude of ionization takes the form

$$\begin{aligned}(S-1)_{fi} &= \frac{1}{i\hbar}\int_{-\infty}^{\infty} dt\left(H_I^{dE}\hat{U}^+\Psi_f^{(-)pA},\Phi_i\right)\\ &= \frac{1}{i\hbar}\int_{-\infty}^{\infty} dt\left(\Psi_f^{(-)dE},H_I^{dE}\Phi_i\right),\end{aligned} \tag{C15}$$

which is identical with the LG result derived in Eq. (C8). In this way, for the exact probability amplitude of ionization, the gauge invariance is preserved. By analogy, starting from Eqs. (C6) and (C10), respectively, and making similar calculations, one can check, that the gauge-invariant direct time form of the S matrix is

$$(S-1)_{fi} = \frac{1}{i\hbar}\int_{-\infty}^{\infty} dt\left(\Phi_f,H_I^{dE}\Psi_i^{(+)dE}\right). \tag{C16}$$

In light of the above calculations it is obvious that the well-known starting point of the VG SFA theory

$$(S-1)_{fi} = \frac{1}{i\hbar}\int_{-\infty}^{\infty} dt\left(\Psi_f^{(-)pA},H_I^{pA}\Phi_i\right) \tag{C17}$$

is not always an exact expression [unless Eq. (C1) is satisfied]. Equation (C17) may be obtained, if one sets $\hat{U}(\vec{r},t) = 1$ during all the time evolution of the ionized electron. This can be deduced from the first line of Eq. (C12) (where we set $\hat{U}^+ = 1$) and Eq. (C8) (where we set $H_I = H_I^{pA}$). However, as we have noted above, $\hat{U}(\vec{r},t) = 1$ is not satisfied in strong laser fields.

In our opinion, the qualitative difference between the so-called LG SFA theories and the so-called VG SFA theories is connected with the matter of gauge invariance. When calculating the probability amplitude of ionization in the S-matrix theory one integrates the time derivative of the overlap $(\Psi_f^{(-)},\Phi_i)$, which is a function of time. As Eq. (C8) clearly shows, such an integration is performed from the point $t = +\infty$, where we know the overlap: $(\Psi_f^{(-)},\Phi_i) = \delta_{fi}$, to the point $t = -\infty$, where this overlap is (analytically) unknown. To obtain an approximate result, we approach the value of the integrand for all times between $t = +\infty$ and $t = -\infty$ by using the Volkov wave function instead of $\Psi_f^{(-)}$. But for any time t obeying $+\infty > t > -\infty$ and $\vec{A}(t) \neq \vec{0}$ the overlap $(\Psi_f^{(-)dE},\Phi_i)$ is the instantaneous probability amplitude of ionization, while the overlap $(\Psi_f^{(-)pA},\Phi_i)$ is not. These two expressions are equal only when $\vec{A}(t) = \vec{0}$. Therefore only in the LG does our approximation have a clear physical

interpretation for all t, which contribute to the analytical value of the integral. Let us note that for the *circularly polarized* laser field (unlike for the linear polarization) one never has $\vec{A}(t) = \vec{0}$, when the laser field has a constant intensity.

[1] E. S. Sarachik and G. T. Schappert, Phys. Rev. D **1**, 2738 (1970).
[2] P. B. Corkum, N. H. Burnett, and F. Brunel, Phys. Rev. Lett. **62**, 1259 (1989).
[3] J. H. Eberly, J. Javanainen, and K. Rzążewski, Phys. Rep. **204**, 333 (1991).
[4] L. V. Keldysh, Zh. Eksp. Teor. Fiz. **47**, 1945 (1964) [Sov. Phys. JETP **20**, 1307 (1965)].
[5] A. M. Perelomov, V. S. Popov, and M. V. Terent'ev, Zh. Eksp. Teor. Fiz. **50**, 1393; **51**, 309 (1966) [Sov. Phys. JETP **23**, 924 (1966); **24**, 207 (1967)].
[6] F. H. M. Faisal, J. Phys. B **6**, L89 (1973).
[7] H. R. Reiss, Phys. Rev. A **22**, 1786 (1980).
[8] J. H. Bauer, J. Phys. B: At. Mol. Opt. Phys. **41**, 185003 (2008).
[9] C. Leone, S. Bivona, R. Burlon, F. Morales, and G. Ferrante, Phys. Rev. A **40**, 1828 (1989).
[10] D. Bauer, D. B. Milošević, and W. Becker, Phys. Rev. A **72**, 023415 (2005).
[11] M. Klaiber, K. Z. Hatsagortsyan, and C. H. Keitel, Phys. Rev. A **73**, 053411 (2006).
[12] W. Becker and D. B. Milošević, Laser Phys. **19**, 1621 (2009).
[13] A. Bechler and M. Ślęczka, Phys. Lett. A **375**, 1579 (2011).
[14] J. Bauer, Phys. Rev. A **73**, 023421 (2006).
[15] J. H. Bauer, Phys. Rev. A **75**, 045401 (2007).
[16] J. H. Bauer, Phys. Scr. **77**, 015303 (2008).
[17] J. H. Bauer, Phys. Rev. A **84**, 025403 (2011).
[18] J. H. Bauer, Phys. Rev. A **79**, 015401 (2009).
[19] W. Gordon, Z. Phys. **40**, 117 (1926)
[20] D. M. Volkov, Z. Phys. **94**, 250 (1935).
[21] X. L. Yang, S. H. Guo, F. T. Chan, K. W. Wong, and W. Y. Ching, Phys. Rev. A **43**, 1186 (1991).
[22] J. H. Bauer and J. Matulewski, Phys. Rev. A **82**, 053418 (2010).
[23] J. H. Bauer (unpublished).
[24] D. B. Milošević, G. G. Paulus, D. Bauer, and W. Becker, J. Phys. B **39**, R203 (2006).
[25] T. K. Kjeldsen and L. B. Madsen, Phys. Rev. A **74**, 023407 (2006).
[26] I. Barth and O. Smirnova, Phys. Rev. A **84**, 063415 (2011).
[27] N. B. Delone and V. P. Krainov, *Multiphoton Processes in Atoms* (Springer Verlag, Berlin, Heidelberg, 1994).
[28] V. P. Krainov, J. Phys. B **32**, 1607 (1999).
[29] M. Gajda, B. Piraux, and K. Rzążewski, Phys. Rev. A **50**, 2528 (1994).
[30] M. Chrysos, J. Phys. B: At. Mol. Opt. Phys. **28**, L373 (1995).